

Geometric Origin of Macroscopic Alignment in Granular Flows

Christopher Harper*

Department of Earth Sciences, University of Oregon, Eugene, USA

Eric C.P. Breard and PJ Zrelak

School of GeoSciences, University of Edinburgh, Edinburgh, UK †

George W. Bergantz

Dept. Earth and Space Sciences, University of Washington, Seattle, USA

(Dated: May 28, 2026)

Predicting the alignment of non-spherical particles in dense granular flows under shear remains a central challenge in soft matter physics. We demonstrate that the first-order behavior of granular fabric, the anisotropic distribution of contacts, is a direct consequence of particle boundary geometry. By assuming uniform contact probability along a particle’s perimeter, we derive a mapping between local curvature and the macroscopic distribution of contact normals. This minimal geometric framework accurately predicts the uniaxial nematic order parameter S_2 observed in both three-dimensional discrete element simulations and laboratory experiments using various particle geometries (e.g, rice, fibers, and disks) across a wide range of aspect ratios. Our results show that particle shape dictates the available orientation statistics, providing a purely geometric baseline for the emergence of fabric in dense granular systems.

INTRODUCTION

The alignment of non-Brownian, nonspherical particles in flow is widely observed in both natural [1–5] and industrial settings [6–8]. This nematic alignment is often referred to as a material “fabric,” or shape-preferred-orientation (SPO). This anisotropic alignment arises in both suspensions and (dry) granular flows, and has been the focus of study from dilute to particle-rich (dense) concentrations [9, 10]. The emergence of fabric can change the packing, strength, and permeability of a multiphase mixture, as it influences the Reynolds dilation, coordination number and the anisotropic distribution of forces and force chain orientation and bulk rheology [11–19]. Hence predicting the terminal orientational and positional ordering in a multiphase mixture of nonspherical particles has significant implications for industrial design and the interpretation of geophysical processes.

It is well established that a particle-rich mixture (dense) under shear will eventually self-organize to what has been called a critical state, where continued shear strain yields no further changes in the volume, shear strength, coordination number or shape preferred orientation (SPO) of the system [20]. This has been demonstrated both experimentally, using material as diverse as rice, grains, glass cylinders, and fibers [21–23] and in numerical simulations [9, 24–26]. One property of the critical state is the emergence of a persistent uniaxial nematic ordering. The strength of the ordering is expressed by the order parameter S_2 , which is the largest eigenvalue of the symmetric traceless order tensor Q (Equation 7) [9, 21].

A value of S_2 equal to unity means all the particle are aligned, and a value of zero means the alignment is isotropic with no preferred orientation. Empirical evidence shows that S_2 is strongly dictated by particle aspect ratio and is remarkably insensitive to realistic values of particle friction [25] or shear rate [21]. While it has been elegantly proposed that this critical state represents a geometrically “saturated” fabric constrained by steric exclusions within the contact network [27], the precise value of S_2 has remained an empirical observation. Despite its reproducibility across various families of shapes, from ellipsoids to flat disks and elongated rods [25], there is currently no first-principles framework to predict the terminal alignment for a given particle assemblage [9].

In this letter we show that the first-order behavior of the orientational distributions arises purely from particle geometry. Our central hypothesis is that the orientational statistics of contact normals are a direct geometric consequence of particle shape, independent of the complex force-chain dynamics or dissipative interaction typically associated with granular flow. By assuming a uniform sampling of particle boundaries, we demonstrate that predictable orientation statistics emerge solely from boundary curvature. This minimal geometric framework provides a physically grounded baseline for understanding the statistical emergence of granular fabric, reconciling the structural limits of the contact network with the fundamental geometry of the particles themselves.

THEORETICAL FRAMEWORK: MAPPING BOUNDARY GEOMETRY TO CONTACT FABRIC

In this section, we establish a purely geometric derivation for the distribution of contact normals in a granu-

* charper4@uoregon.edu

† Department of Earth Sciences, University of Oregon

lar assembly. We hypothesize that for a given particle shape, the local boundary curvature dictates the statistical likelihood of contact at any given orientation. This geometric mapping arises because each particle-particle contact defines a branch vector and an associated contact normal, which together encode the local fabric of the material. Because forces and torques are transmitted through these contacts, admissible particle orientations are restricted to those compatible with the geometry of the surrounding contact network.

By assuming the contacts are uniformly distributed along a particle's perimeter, we derive a minimal description of how boundary curvature constrains these normal orientations. This approach isolates the role of particle geometry from the dynamical complexities of force transmission and dissipation, allowing us to show that this purely geometric constraint captures the dominant features of the observed orientational statistics.

To isolate the role of geometry, we make three simplifying assumptions:

1. **Particle shape:** Particles are convex, with boundaries approximated by either smooth (ellipsoids) or piecewise-smooth (rectangles) geometries.
2. **Planar confinement:** Under steady simple shear, alignment occurs predominantly within the shear plane; out-of-plane fluctuations are neglected.
3. **Geometric control:** Within the shear plane, orientation statistics are determined primarily by geometry, with dynamics entering only through contact formation.

Given the assumptions above, the role of particle boundary curvature in setting the contact distribution simplifies to the two-dimensional perimeter curvature within the shear plane. Contact locations are then modeled as uniformly distributed with respect to this perimeter arc length s , such that the probability that any point is a contact point, $p(s)$, is constant over the perimeter. However, this uniform distribution of particle contacts does not imply a uniform distribution of normal orientations.

Each point along the boundary is associated with a unique outward normal, whose direction we parameterize by the polar angle θ in the shear plane. The map from arc length s to orientation angle θ defines a change of variables between probability measures. Applying the standard relation,

$$P(\theta) = p(s) \left| \frac{ds}{d\theta} \right|,$$

we see that the orientational distribution is governed by the geometric factor $|ds/d\theta|$, which measures how much boundary length contributes to a given angular interval of the normal.

This quantity is directly related to the curvature κ of the boundary,

$$\frac{ds}{d\theta} = \frac{1}{\kappa}.$$

Thus,

$$P(\theta) \propto \frac{1}{\kappa(\theta)}. \quad (1)$$

To evaluate this explicitly, we consider an ellipse with semi-axes a and b , the points along the boundary are parameterized by

$$r(\phi) = (a \cos \phi, b \sin \phi),$$

where ϕ is the standard parametric angle. The curvature as a function of ϕ is

$$\kappa(\phi) = \frac{ab}{(a^2 \sin^2 \phi + b^2 \cos^2 \phi)^{3/2}}. \quad (2)$$

Each point also defines a unique outward normal. As before θ , denotes the polar angle of this normal. The geometric relation between ϕ and θ is

$$\theta = \arctan \left(\frac{a}{b} \tan \phi \right).$$

Using this transformation, we express the curvature with respect to the normal orientation:

$$\kappa(\theta) = \frac{(a^2 \cos^2 \theta + b^2 \sin^2 \theta)^{3/2}}{a^2 b^2}. \quad (3)$$

In this form, curvature acts as a geometric weight on the likely orientations of contact normals, and because contact normals determine the torque balance on a particle, this distribution provides a direct geometric proxy for the statistically preferred particle orientations.

Figure 1 illustrates how $P(\theta)$ varies with aspect ratio. With the analytical form $P(\theta) \propto 1/\kappa(\theta)$, we generate predicted orientation distributions for ensembles of ellipsoidal grains, including both prolate and oblate shapes.

To demonstrate the generality of the curvature-based framework, we consider the limiting case of a rectangular particle in the shear plane. In contrast to smooth shapes such as ellipses, a rectangle consists of flat edges separated by sharp corners. Along each flat edge, the outward normal direction is constant, while at the corners the curvature is infinite.

Because contact normals are defined up to a sign, we restrict orientations to $\theta \in [0, \pi)$, identifying θ and $\theta + \pi$. Under this convention, a rectangle with edge lengths w (horizontal) and h (vertical) admits only two distinct normal orientations:

$$\theta \in \left\{ 0, \frac{\pi}{2} \right\}.$$

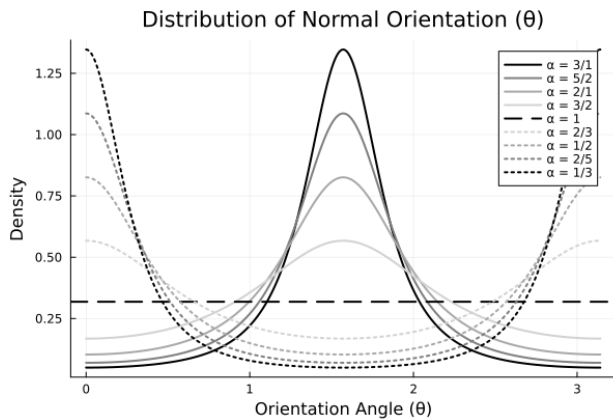


FIG. 1. Geometric warping of contact-normal orientations by particle shape. For a circular particle ($\alpha = 1$), uniform sampling along the boundary yields a uniform distribution of contact-normal orientations $P(\theta)$. As the aspect ratio deviates from unity, the distribution becomes more biased.

Assuming uniform sampling of contact locations along the boundary, the probability of observing a given orientation is proportional to the total length of edges sharing that normal. With total perimeter $L = 2w + 2h$, this yields the discrete distribution

$$P(\theta) = \begin{cases} \frac{2h}{L}, & \theta = 0, \\ \frac{2w}{L}, & \theta = \frac{\pi}{2}, \\ 0, & \text{otherwise.} \end{cases} \quad (4)$$

To better understand in what ways rectangles represent a limiting form of the ellipsoid geometry, we represent the distribution as a sum of Dirac delta functions,

$$P(\theta) = \frac{2h}{L} \delta(\theta) + \frac{2w}{L} \delta\left(\theta - \frac{\pi}{2}\right), \quad \theta \in [0, \pi). \quad (5)$$

This form makes the orientation distribution's concentration at the face normals explicit, weighting it by the relative edge lengths. It can be understood as the singular limit of the continuous relation $P(\theta) \propto 1/\kappa(\theta)$: along the flat edges $\kappa \rightarrow 0$, leading to a concentration of probability, while at the corners $\kappa \rightarrow \infty$, yielding negligible contribution. To illustrate this geometric collapse, Figure 2 contrasts the continuous orientation distribution of an ellipsoid with the discrete probability mass of a rectangle of the same aspect ratio (3:1). For the rectangle, the shaded domains do not represent a continuous spread of normal angles; rather, the width and area of the shaded bins represent the total probability mass (proportional to the flat edge lengths) that collapses entirely onto the discrete face normals (e.g., the long edge mapping exactly to $\theta = \pi/2$).

The rectangular case emerges as a limiting form in which a continuous spectrum of orientations collapses onto a discrete set. Although a pathological extreme of our curvature argument, such piecewise-continuous geometries are physically relevant, appearing in the rect-

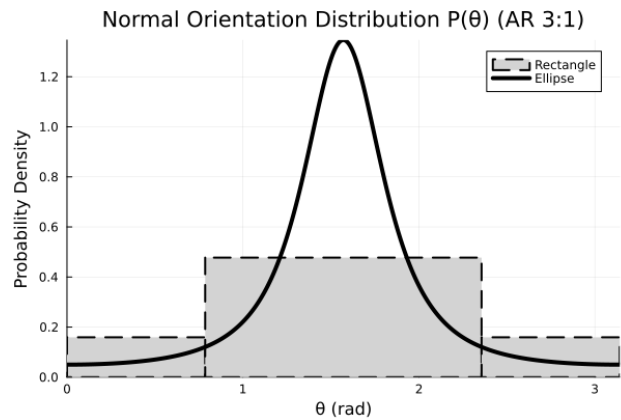


FIG. 2. Comparison of normal orientation distributions for smooth versus piecewise-flat boundaries. The solid curve represents the continuous probability density $P(\theta)$ for an ellipsoid with an aspect ratio of 3:1. The shaded regions represent the distribution for a rectangle of the same aspect ratio.

angular cross-sections of cylindrical simulations and the faceted surfaces of fragmented natural materials.

While these distributions are derived from a single-particle geometric model, their predictive power extends to dense systems. The following section details this extension.

METHODS: CONSTRUCTING THE STATISTICAL ENSEMBLE FOR MACROSCOPIC ALIGNMENT

For any ellipsoidal particles, we can generate the analytical expression for $\kappa(\theta)$ (Equation 3) from the major and minor axes of the ellipse formed by projecting the ellipsoidal onto the shear plane. The probability density function $P(\theta)$ is the normalized reciprocal of this function as shown in Equation 6. While $P(\theta)$ is not a standard distribution, its exact analytical form makes it an ideal candidate for rejection sampling, whereby random candidate angles are uniformly generated and then accepted or discarded based on whether an independent uniform random variable falls below the evaluated probability density $P(\theta)$. Therefore we generate 2,000 orientations sampled from $P(\theta)$ through rejection sampling, and we will call this list of two-thousand orientations Θ . The sample size of 2,000 is somewhat arbitrarily chosen to reflect sampling one contact normal per particle in the Bilotto simulations, to which we compare our results.

$$P(\theta) = \frac{f(\theta)}{\int_0^\pi f(\theta) d\theta}, \quad \text{where } f(\theta) = \frac{1}{\kappa(\theta)} \quad (6)$$

Sampling for the rectangular particles is similar, however, we don't use an exact expression for $P(\theta)$ to perform rejection sampling, but rather, we directly simulate

the uniform perimeter-based sampling which arises from Equation 4.

To calculate S_2 we first build our orientation tensor following standard conventions for granular nematics [9, 21]. For each sampled θ in Θ , we define a two-dimensional unit orientation vector \hat{u}_n (restricted to the shear-plane) such that $\hat{u}_n = (\cos(\theta_n), \sin(\theta_n))$. The macroscopic alignment is quantified using the standard symmetric, traceless nematic orientation tensor, Q . The bulk tensor is computed as the ensemble average over all N particles. In Equation 7 I is the dimensional identity matrix, and \otimes denotes the outer product.

$$Q = \frac{1}{N} \sum_{n=1}^N \left(\hat{u}_n \otimes \hat{u}_n - \frac{1}{2}I \right) \quad (7)$$

Because Q is a real, symmetric tensor, we can determine its principal directions of alignment by computing its eigenvalues. The eigenvector associated with the largest eigenvalue represents the dominant macroscopic orientation. Let λ_{max} be the maximum eigenvalue of the ensemble-averaged Q tensor, then this eigenvalue serves as a single scalar metric which quantifies the strength of the macroscopic alignment. Scaling λ_{max} by 2 we arrive at the uniaxial nematic order parameter, S_2 :

$$S_2 = 2\lambda_{max} \quad (8)$$

This scaling normalizes the order parameter to the standard bounds introduced earlier, mapping the isotropic state ($\alpha = 1$) to $S_2 = 0$ and the perfectly nematic state to $S_2 = 1$. By extracting this scalar metric from our sampled ensembles, we establish a direct, quantitative link between the localized geometric warping of $P(\theta)$ and macroscopic fabric anisotropy.

RESULTS

We apply our geometric framework to predict the uniaxial nematic order parameter, S_2 , across a wide range of ellipsoidal aspect ratios ($\alpha \in [0.1, 10]$). These predictions are compared against three-dimensional, frictional discrete element method (DEM) simulations from Bilotto et al. [9] and laboratory experiments using rice grains by Börzsönyi et al. [21]. To facilitate comparisons across different studies we convert all aspect ratios (a/b) into a shape ratio ($R_g = (a-b)/(a+b)$).

As shown in Figure 3, the geometric model closely follows the results of highly frictional systems ($\mu = 1.0$) and successfully captures the general envelope of the DEM data of Bilotto et al [9]. The experimental alignment of rice grains also aligns well with our geometric baseline, despite decadal variations in shear rate. These results suggest that while friction and kinematics modulate the magnitude of alignment, the first order behavior of granular fabric is fundamentally dictated by the warping of contact probability due to boundary curvature.

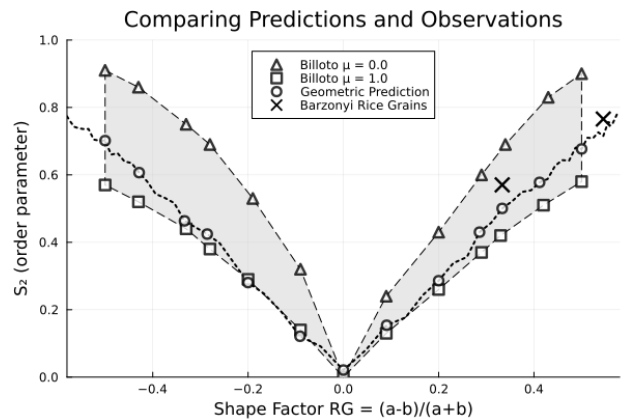


FIG. 3. Comparison of geometric predictions with numerical and experimental data. The uniaxial nematic order parameter S_2 is plotted against the shape ratio $R_g = (a-b)/(a+b)$. Our analytical prediction (dotted line) identifies specific values for ellipsoidal geometries (circles). The shaded region represents the envelope of outcomes from DEM simulations by Bilotto et al.[9], ranging from frictionless ($\mu = 0.0$, upper bound) to highly frictional ($\mu = 1.0$, lower bound) systems. Crosses (X) denote experimental results for rice grains of aspect ratios 2.0 and 3.4, averaged across shear rates from 0.01 to 1.0 s^{-1} (adapted from Börzsönyi et al.[21])

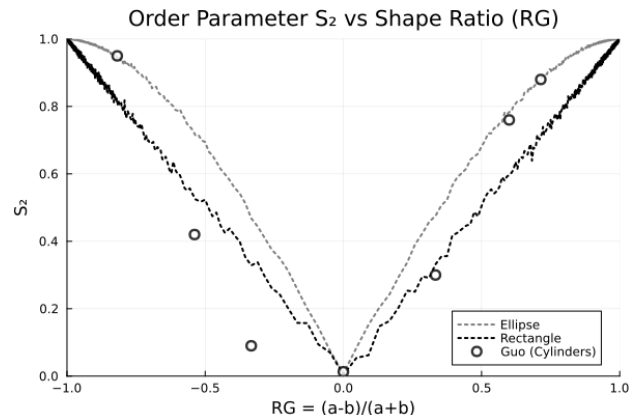


FIG. 4. Geometric model performance across distinct particle classes. Comparison of S_2 predictions for smooth ellipsoids (dotted line) and piecewise-flat rectangles (dashed line) against data for cylinders and disks (open circles) from Guo et al. [25]

When considering a different class of particle geometries (disks and rods with planar surfaces), the results are less clear. For these particles, we utilize the rectangular model derived in Equation 5. As illustrated in Figure 4, the rectangular cross section better describes disks and rods of intermediate to low aspect ratios, however for more extreme aspect ratios the simulations almost snap onto the elliptical predictions.

DISCUSSION

The emergence of a stable shape-dependent alignment in the critical state has previously been described as a “geometric saturation”. In this framework Radjaï et al. [27] proposed that the contact anisotropy is bounded by available spaces of accessible fabric states; however, the precise value of this saturation point has remained an empirical observation dependent on specific material properties. Our framework provides a physical basis for these states by demonstrating that the steady-state distribution of contact normals is mapped directly from the particle’s boundary curvature. By identifying the geometric weight $1/\kappa(\theta)$ as the primary driver of contact normal density, we provide a predictive link between particle geometry and these fabric limits, effectively grounding “accessible states” in the fundamental curvature of the particle boundary.

Recent work by Marschall et al. [28] examined the surface probability distribution of contacts $P(\vartheta)$, in sheared assemblies of frictionless ellipsoids and spherocylinders, demonstrating that contacts preferentially localize along the narrowest particle widths near jamming. Their results provide an important complementary perspective to the present framework. In their formulation, $P(\vartheta)$ characterizes the dynamical bias governing where contacts occur on the particle surface, arising from shear-induced stress anisotropy and collision dynamics. Here, by contrast, we isolate the purely geometric contribution by asking how any distribution of surface contacts maps into a distribution of contact-normal orientations. Under the assumption of uniform boundary sampling, this mapping reduces to the curvature weighting $P(\theta) \propto 1/\kappa(\theta)$. In this sense, the present model does not attempt to describe the full dynamical process of contact formation, but instead establishes the geometric transform linking boundary geometry to orientational statistics. The close agreement between this minimal construction and both DEM simulations and laboratory measurements suggests that much of the observed nematic alignment may emerge from geometric constraints intrinsic to particle shape, with dynamics acting primarily as a modulation of this underlying geometric bias. This distinction between geometric constraints and dynamical modulation may also help explain why different particle classes exhibit varying degrees of agreement with the smooth-curvature predictions developed here.

An intriguing observation in our comparison between the geometric models and the DEM data from Guo et al. [25] is the transition of cylinders, which possess rectangular cross-sections, from following the discrete rectangle prediction at moderate aspect ratios to aligning with the continuous elliptical prediction at larger aspect ratios. We suspect this alignment with ellipses occurs because of an additional effect where a small tilt out of the shear plane creates an elliptical cross-section within the shear plane. For the same angle of tilt, this effect becomes more pronounced for shape values R_g further

from zero. Furthermore, while the potential for planar contacts alters the nature of contact availability and the driving dynamics of the system, in a dense packing of highly elongated rods, flat ends are effectively shielded. This makes planar interactions highly improbable compared to contacts along the elongated sides. Because even a slight out-of-plane tilt effectively introduces non-zero curvature into the shear plane, future work examining the fully three-dimensional kinematics of faceted and planar shapes would be highly valuable. Despite these three-dimensional nuances, the capacity of this framework to capture the behavioral bounds of such extreme geometries points to a much broader applicability of the curvature-based model.

This broader applicability is supported by the findings of Börzsönyi et al. [21], who observed robust, shape-dependent macroscopic alignment across diverse laboratory materials—not just in strictly elliptical rice grains, but also in non-elliptical glass cylinders. Furthermore, it is well established that micro-structural organization in these systems is fundamentally driven by collision events [22]. Crucially, the orientational bias generated by these collisions is dictated by the distribution of branch vectors formed during impact. Because the available branch vectors are mapped directly from the geometry of the particle boundary, the fundamental curvature of the particle remains an essential driver of fabric anisotropy.

More broadly, because the present argument is geometric, it should remain relevant across dense particulate flows spanning dry-granular and viscous-suspension regimes, provided the system is sufficiently particle-rich and experiences sustained particle contacts. For instance, in crystal-rich magmas, this same geometric constraint may therefore provide a useful baseline for illuminating the development of crystal fabric and lineation. The data used for validation in this work shows that the quasi-static state is sufficient to meet these conditions. Of future interest would be to explore whether or not it is necessary, as the work of Börzsönyi et al. [21] suggest that similar alignment behavior may persist beyond the quasi-static regime. We expect, however, that as inertial effects become increasingly important, geometric controls will progressively lose predictive power.

CONCLUSION

We have demonstrated that the first-order alignment of non-spherical particles in dense granular flow can be predicted from a purely geometric consideration of particle boundary curvature. By mapping the local curvature to a probability distribution of contact normals, we recover the macroscopic fabric anisotropy observed in complex three-dimensional DEM simulations across a wide range of particle aspect ratios.

Our model assumes uniform contact probability along the perimeter, and its success suggests that geometric constraints are the dominant factor in determining

steady-state fabric. This purely geometric baseline successfully reconciles previous theoretical hypothesis of ‘geometric saturation’ in granular contact networks with empirical observations of diverse analog laboratory experiments [21, 27]. Future refinements could incorporate kinematic effects, such as the tumbling behavior of particles with extreme aspect ratios, or extend the framework to include non-uniform contact distributions driven by specific flow configurations. Nevertheless, this minimal geometric framework provides a robust baseline for predicting the statistical emergence of granular fabric in multiphase systems.

ACKNOWLEDGMENTS

Financial support was provided to C.H. by NSF EAR Postdoctoral Fellowship award No. 2518495. This research was also supported in part by grant NSF PHY-2309135 to the Kavli Institute for Theoretical Physics (KITP), whose unique environment facilitated the origins of this work. E.C.P.B. was supported by the NERC-IRF (NE/V014242/1), the Leverhulme Trust grant award RPG-2024-294 and the Royal Society (IEC/NSFC/242381). Financial support was also provided to P.Z. by the Leverhulme Trust grant award RPG-2024-294.

-
- [1] L. Arbaret, H. Diot, and J.-L. Bouchez, *Journal of Structural Geology* **18**, 941 (1996).
- [2] K. E. Ardill, S. R. Paterson, J. Stanback, P. H. Alasino, J. J. King, and S. E. Crosbie, *Frontiers in Earth Science* **8**, 10.3389/feart.2020.00190 (2020).
- [3] B. Latimer, W. McCarthy, T. Mattsson, and J. Reavy, *Geosphere* **20**, 1390 (2024).
- [4] S. R. Paterson, K. Ardill, R. H. Vernon, and J. Žák, *Journal of Structural Geology* **125**, 134 (2019).
- [5] J. Žák, K. Verner, and P. Týcová, *Geological Magazine* **145**, 537 (2008).
- [6] T. Börzsönyi and R. Stannarius, *Soft Matter* **9**, 7401 (2013).
- [7] B. Fan, T. Pongó, R. Cruz Hidalgo, and T. Börzsönyi, *Physical Review Letters* **133**, 058201 (2024).
- [8] F. Fernández-Gil and J. Leyrer, *Polymer Composites* 10.1002/pc.70627 (2025).
- [9] J. Bilotto, M. Trulsson, and J.-F. Molinari, *Physical Review E* **112**, 045432 (2025).
- [10] A. Okagawa, R. G. Cox, and S. G. Mason, *Journal of Colloid and Interface Science* **45**, 303 (1973).
- [11] P. Adesina, C. O’Sullivan, and T. Wang, *Computational Particle Mechanics* 10.1007/s40571-023-00632-8 (2023).
- [12] E. Azéma and F. Radjai, *Physical Review E* **81**, 051304 (2010).
- [13] E. Azéma, F. Radjai, B. Saint-Cyr, J.-Y. Delenne, and P. Sornay, *Physical Review E* **87**, 052205 (2013).
- [14] T. Börzsönyi, E. Somfai, B. Szabó, S. Wegner, P. Mier, G. Rose, and R. Stannarius, *New Journal of Physics* **18**, 093017 (2016).
- [15] J. E. Butler and B. Snook, *Annual Review of Fluid Mechanics* **50**, 299 (2018).
- [16] J. Guo, Q. Zhou, and R. C.-K. Wong, *Physics of Fluids* **33**, 10.1063/5.0059346 (2021).
- [17] M. Trulsson, *Journal of Fluid Mechanics* **849**, 718 (2018).
- [18] Y. Zou, G. Ma, J. Mei, J. Zhao, and W. Zhou, *Acta Geotechnica* **17**, 2697 (2022).
- [19] Y. Zou, G. Ma, S. Zhao, S. Chen, and W. Zhou, *Powder Technology* **416**, 118235 (2023).
- [20] F. Radjai and E. Azéma, *European Journal of Environmental and Civil Engineering* **13**, 203 (2009).
- [21] T. Börzsönyi, B. Szabó, G. Törös, S. Wegner, J. Török, E. Somfai, T. Bien, and R. Stannarius, *Physical Review Letters* **108**, 228302 (2012).
- [22] S. Strednak, J. E. Butler, L. Bergougnoux, and E. Guazzelli, *Physical Review Fluids* **6**, 014302 (2021).
- [23] S. Wegner, T. Börzsönyi, T. Bien, G. Rose, and R. Stannarius, *Soft Matter* **8**, 10950 (2012).
- [24] D. Z. Gunes, R. Scirocco, J. Mewis, and J. Vermant, *Journal of Non-Newtonian Fluid Mechanics* **155**, 39 (2008).
- [25] Y. Guo, C. Wassgren, B. Hancock, W. Ketterhagen, and J. Curtis, *Physics of Fluids* **25**, 063304 (2013).
- [26] S. Zhao, J. Zhao, and N. Guo, *Physical Review E* **101**, 012906 (2020).
- [27] F. Radjai, J.-Y. Delenne, E. Azéma, and S. Roux, *Granular Matter* **14**, 259 (2012).
- [28] T. Marschall, Y.-E. Keta, P. Olsson, and S. Teitel, *Physical Review Letters* **122**, 188002 (2019).